

Caspian Sea ocean model

M. Gunduz E. Özsoy

Title Page

Abstract

Introduction

Conclusions

References

Tables

Figures

◀

▶

◀

▶

Back

Close

Full Screen / Esc

Printer-friendly Version

Interactive Discussion



a cumulative indicator of a series of other changes leading up to possible regime shifts between alternative states of the ecosystem. Large variations have been observed in winter mixing, varying from shallow to deep convection, with strong cases of deep ventilation (Kosarev and Yablonskaya, 1994; Dumont, 1998). In one such case following the abrupt drop of sea level in 1977, dramatic changes in stratification and nutrient regimes are known to have occurred (Kosarev and Yablonskaya, 1994).

Like the neighboring Black Sea, the Caspian Sea is an enclosed basin with large fresh water inputs from rivers, the most significant such contribution being from the Volga, among others such as the Ural, Kura and Terek. Input from rivers are known to be capable of creating buoyancy driven shelf currents, as shown by a number of detailed studies (e.g. Kourafalou et al., 1996; Lazure and Jegou, 1998; Chen et al., 1999).

It is challenging to capture and to explain the observed complex features of the Caspian Sea circulation arising from wind and atmospheric/riverine buoyancy forcing acting on this elongated, enclosed sea, and worthwhile to study the rather large contrasts between its basins, the variability of flow and mixing processes along its coasts.

The general circulation inferred from hydrographic survey data from the end of the 19th century till the 1950s has been described to be cyclonic in the Middle Caspian Sea (MCS). Instrumental surveys along the western coast of the MCS, carried out in 1935–1937 (Stockman, 1938; Baidin and Kosarev, 1986), have shown predominantly southward currents along the western coast of the basin. Data from oceanographic observations since the 1950's in coastal areas have confirmed southward currents along the western coast of the MCS (Klevtsova, 1967) and a semi-permanent anticyclonic vortex south of the Apsheron peninsula (Tsytzarev, 1967). Southward surface currents along the eastern coast of the MCS (Klevtsova, 1967; Bondarenko, 1993) evident in these observations at first seem to contradict the above mentioned general cyclonic circulation of the MCS. However, below this depicted surface circulation, northward currents with seasonal variation are known to exist along the eastern coast of the basin, supporting the proposed cyclonic circulation (Kosarev and Yablonskaya, 1994).

Caspian Sea ocean model

M. Gunduz E. Özsoy

Title Page

Abstract

Introduction

Conclusions

References

Tables

Figures

◀

▶

◀

▶

Back

Close

Full Screen / Esc

Printer-friendly Version

Interactive Discussion



A southward current east of the Apsheron peninsula passing to the South Caspian Sea (SCS) have been inferred from hydrographic observations, with current speed of $50\text{--}60\text{ cm s}^{-1}$ at the surface, decreasing to $40\text{--}50\text{ cm s}^{-1}$ near the bottom (Kosarev and Yablonskaya, 1994). By making use of satellite derived SST and chlorophyll data, (Sur et al., 2000) have revealed the southward flow of cold water from the north along the west coast, and the northward intrusion of warm water from the SCS to the MCS near the eastern coast. In the shallow North Caspian Sea (NCS), the circulation appears to be almost totally controlled by local winds (Bondarenko, 1993; Terziev et al., 1992). Based on the above mentioned features, (Lednev, 1943) have created the schematic representation of the Caspian Sea circulation shown in Fig. 1.

The construction of the missing elements of the above description of seasonal circulation hopefully could be achieved by details supplied by numerical model studies performed since the mid-1970s till present. The diagnostic model developed by (Sarkisyan et al., 1976) indicated a mainly wind driven circulation, and the effects of thermal stratification in establishing this circulation. Diagnostic models of Trukhchev et al. (1995) and Tuzhilkin et al. (1997) have indicated dipole structures, respectively consisting of a cyclonic and anticyclonic pair in the northwest and southeast of the MCS, and an anticyclonic and cyclonic pair in the northwest and southeast of the SCS basins.

Later, a review and a series of computations of the seasonal circulation based on a coupled sea hydrodynamics, air/sea interaction and sea ice thermodynamics model of the Caspian Sea have been made by Ibrayev et al. (2010) establishing the importance of seasonal changes from cyclonic to anticyclonic circulation patterns, topographic generation and steering of currents along the eastern and western coasts. A persistent northward transport by subsurface currents was shown along the eastern shelf slope, despite the often southward directed surface currents in the same region, confirming the features reviewed above, as well as displaying horizontally and vertically layered structure of the boundary currents over a mild slope. Recently, by assimilating climatological temperature and salinity into a primitive-equation ocean circulation model, Knysh et al. (2008) have obtained a cyclonic circulation in the MCS in winter,

with the above mentioned features of a southward surface current and a northward sub-surface current along the eastern shelf. Knysh et al. (2008) have found a highly variable circulation corresponding to an intense, mostly barotropic circulation in February, and a relatively less intense baroclinic circulation in the March–June period.

Faced with an insufficient understanding of the circulation and its various details hidden in the existing knowledge, our primary focus is to re-create the 3-D seasonal circulation under climatological wind, surface and river buoyancy forcing, to discover basin-wide features and meso-scale details and check their consistency with available observations.

2 Bathymetry

Each of the three basins of the Caspian Sea has distinct physical and biological properties (Fig. 2). The NCS is extremely shallow, with an average depth of about 5 m, the Ural Furrow of 8–10 m depth cutting through the otherwise flat region. The NCS is separated from the MCS by an abrupt depth transition at the shelf edge. The depth in the MCS is about 190 m on the average, reaching a maximum value of 788 m at the Derbent depression on its western side. The western slope of the MCS is quite steep, whereas the eastern slope is milder. The Kara Boğaz Göl, a small enclosure with less than 10 m depth, originally connected to the Caspian Sea, and adjacent to the eastern deserts has recently been dammed to reduce water losses from the Caspian Sea by evaporation. The deep basins of the MCS and the SCS are separated by the Apsheron sill of 150 m maximum depth. The SCS is the deepest basin, with a maximum depth of 1025 m and shallower depressions of 900 to 1000 m depth. The wide continental shelf extending along the eastern side of the SCS is connected to the narrow shelf continuing along the eastern side of the MCS.

Title Page

Abstract

Introduction

Conclusions

References

Tables

Figures

◀

▶

◀

▶

Back

Close

Full Screen / Esc

Printer-friendly Version

Interactive Discussion



3 Model features and setup

Features of the Caspian Sea, such as the weak stratification, deep mixing, and strong topographic gradients at continental slopes and sills make the HYbrid Coordinate Ocean Model (HYCOM) (Bleck, 2006) ideally suited for our studies.

The HYCOM, a generalized (hybrid, isopycnal/terrain-following σ/z -level) coordinate primitive equation model, has been widely used for global and regional studies and tested for performance. To cite a few recent studies, the choices of vertical coordinates have been evaluated in the Atlantic Ocean by Chassignet et al. (2003); performance in the Kuroshio Extension region has been tested by Kelly et al. (2007); and the sensitivity to atmospheric forcing in the Black Sea has been investigated by Kara et al. (2005).

The hybrid coordinates extend the range of applicability of the model so as to allow better representation of shallow coastal or weakly stratified waters. The transition from isopycnal coordinates in stratified water to fixed depth z -levels in unstratified surface mixed layer and to terrain-following σ -levels in shallow water occurs smoothly by making use of a layer continuity equation (Bleck, 2002).

A Mercator grid (204×354) with meridional resolution of 4.4 km and zonal resolution of $0.04 \times \cos(\text{lat}) \times 111.2$ km corresponding to 3.0–3.3 km is used. 30 hybrid layers consisting of 14 sigma levels to a depth of 50 m and 16 z -levels below are used in the vertical.

River runoff is first added to a single ocean grid point and smoothed over surrounding ocean grid points, treated as a contribution to precipitation. Monthly discharges of the Volga River, which accounts for about 80% of the climatological mean river discharge of $250 \text{ km}^3 \text{ yr}^{-1}$ (Kosarev and Yablonskaya, 1994), and the two other major rivers Ural and Kura are applied, based on the RivDIS climatology (Vorosmarty et al., 1997). Table 1 shows the monthly discharge of the rivers from RivDIS data set. The peak discharges of these rivers typically occur in April–July, decreasing during November–December. Exchange with Kara-Boğaz Göl, currently disconnected from the Caspian Sea has not been taken into consideration.

OSD

11, 259–292, 2014

Caspian Sea ocean model

M. Gunduz E. Özsoy

Title Page

Abstract

Introduction

Conclusions

References

Tables

Figures

◀

▶

◀

▶

Back

Close

Full Screen / Esc

Printer-friendly Version

Interactive Discussion



Caspian Sea ocean model

M. Gunduz E. Özsoy

Title Page

Abstract

Introduction

Conclusions

References

Tables

Figures

◀

▶

◀

▶

Back

Close

Full Screen / Esc

Printer-friendly Version

Interactive Discussion



The gridded temperature and salinity climatological data ($0.25^\circ \times 0.2^\circ$ resolution and 0, 5, 10, 15, 20, 25, 30, 50, 75, 100, 125, 150, 200, 250, 300, 400, 500, 600, 800 m depth levels) of Ibrayev et al. (2001) are used to initialize the model, after interpolation to the model grid.

The atmospheric forcing is based on the seasonal average ERA-40 (resolution $1.125^\circ \times 1.125^\circ$) of the European Centre for Medium-Range Weather Forecasts (ECMWF), encompassing 40 yr of data 1958–1998. The surface forcing climatology is constructed for the following variables; zonal and meridional components of wind stress, wind speed at 10 m above the sea surface, air temperature, air mixing ratio at 2 m above the sea surface, precipitation, net shortwave radiation and net longwave radiation. The high frequency (6-hourly) component has then been added to the wind stress in the same way as described by Wallcraft et al. (2003), choosing data from the September 1994–September 1995 period as a typical year that would most closely match annual cyclicality in winds.

The model is initialized with monthly mean temperature and salinity climatology and forced with climatological mean seasonal wind stress and surface heat fluxes, with surface salinity relaxed to the observed seasonal mean values. A run period of about 8 model years was sufficient to reach statistical equilibrium, (i.e., a perpetual annual cycle, with negligible temporal drift). The model results presented in the following sections are based on either daily or monthly means that were constructed from the last 4 yr of the simulations.

4 Seasonal circulation

Figure 3 (upper) shows the annual mean circulation of the Caspian Sea averaged over the 0–30 m, 30–150 m, 150–300 m depth intervals. Annual mean currents are generally found to be weak, with maximum values of $7\text{--}8\text{ cm s}^{-1}$ along coastal areas. Although surface currents driven by daily winds display significant variability, this is not reflected in the annual average circulation.

Caspian Sea ocean model

M. Gunduz E. Özsoy

Title Page

Abstract

Introduction

Conclusions

References

Tables

Figures

◀

▶

◀

▶

Back

Close

Full Screen / Esc

Printer-friendly Version

Interactive Discussion



transporting warm water of the southern basin to the north. This northward current is evident from satellite SST data, often as a vein of warm water originating from the SCS flowing towards the MCS along the eastern coast as evident in the satellite derived SST. The sill topography appears to be an important factor controlling the exchange between the two basins, which in turn responds to the structure of the seasonal circulation in the adjacent basins.

In the South Caspian Sea, a persistent dipole pattern and a basin-wide cyclonic circulation trapped along the 100–300 m bathymetric contours are observed. The cyclonic shallow circulation encircles the inner basin dipole pattern. Of the dipole structure, the cyclonic cell is located in the southwestern part of the basin, while the anticyclonic cell is located to its north. The anticyclonic cell, identified as the “Kura anticyclone” by Trukhchev et al. (1995) and Tuzhilkin et al. (1997), has first been described by Lednev (1943). These authors have also found the cyclonic cell in the southeastern part of the SCS. The dipole pattern is a permanent feature of the SCS, evident during the whole year, with mainly barotropic structure extending from the surface to the bottom. The southward current originating from the MCS passes the sill offshore of the Apsheron peninsula, progressing in the form of a coastal jet along the western coast of the SCS. This coastal current reaches its maximum intensity after becoming confined to the steep inner shelf along the west coast of the SCS. The coastal jet follows the shallow bathymetry to turn clockwise around the SCS along the 100–300 m bathymetric contours of the continental slope, finally arriving at the eastern side of the Apsheron sill. Outside this cyclonic circulation cell, southerly flow occurs on the wide eastern continental shelf of the SCS. The double gyre SCS seasonal circulation appears more stable compared to the circulation patterns in the other two basins of the Caspian Sea, in confirmation of Peeters et al. (2000), who showed enhanced vertical stability of this basin, based on Brunt-Väisälä frequency.

December and August monthly mean currents averaged over depth intervals of 0–30 m, 30–150 m, 150–300 m, are plotted in Fig. 3 middle and lower respectively to represent winter and summer regimes of circulation. A cyclonic surface circulation

of the western coast, only to be interrupted by the sharp protrusion of the Apsheron peninsula. The circulation along the wider continental shelves and continental slopes of the corrugated eastern coast (see Fig. 2) are more complex, showing a reversal of direction in the vertical, and complicated horizontal structure. The general circulation appears to be mainly wind driven, while sources of buoyancy also play significant roles.

5 Mesoscale circulation

The above described coastal jets and intense circulation cells often become unstable and create eddies and other meso-scale activity responsible for local mixing and transport. A similar role of the rim current is well known in the case of the neighboring Black Sea (Rachev and Stanev, 1997). The circulation elements also influence pre-conditioning for wintertime convection contributing to deep/intermediate water formation.

Model derived and satellite detected sea surface temperature (SST), height (SSH), salinity (SSS) and other fields are often dominated by meso-scale features with patterns that are quite different from the mean circulation patterns discussed in the last section. While the mean fields are dominated by the coastal jets, rim currents and basin-scale gyres, the snapshots are dominated by eddies with horizontal scales of 10–100 km, especially in the upwelling region, along the coastal boundaries and near dense water formation sites.

Figure 4 shows 0–30 m average currents in the MCS for the month of July, where a complex pattern of basin circulation is displayed, together with intense southerly coastal jet flows along the western and northeastern coasts. While the flow along the western coast is a relatively steady feature of the circulation, the jet flow near the eastern coast of the MCS which later separates from the coast towards the south is a seasonal feature that starts forming in June and continues to intensify by August. At the headland just north of 43° N on the eastern coast, the flow separates from the coast to divide into two branches: while one branch turns to the north and follows the

Title Page

Abstract

Introduction

Conclusions

References

Tables

Figures

◀

▶

◀

▶

Back

Close

Full Screen / Esc

Printer-friendly Version

Interactive Discussion



of mesoscale eddies, wave-like oscillations and filaments. These features in Fig. 7 correspond to a rich field of meso-scale activity.

There are a few modifications in the course of time to the rim current and the embedded simple three cell circulation of the SCS outlined above. The cyclonic and anticyclonic sub-basin gyres display important changes in size and strength, and as shown in Fig. 7e the southern cyclonic gyre at times extends to take over part of the anticyclonic circulation to its north, later to recede south. The circulation interacts with the coast and reversals of currents occur in shallow areas landward of the continental slope. Such reversals occur in the northwest coastal sector of the SCS, particularly near the headland around 50.2° E, 37.5° N, leading to the development of an anticyclonic vortex near 52° E, 37° N sheltered from the cyclonic gyre. The flow along the eastern shelf is also highly variable. The intense southerly flow observed in the shallow inner shelf of the southeastern corner in Fig. 7a–c later becomes organized in the form of an anticyclonic gyre east of the continental slope marked by the 100–300 m depth contours in Fig. 7d–f. The region outside the inner shelf, but east of the continental slope displays numerous small eddies and oscillating currents most of the time, and especially when the anticyclonic eddy in the southeast is not present.

Some of the above described features are easily detected from satellite data. Chlorophyll concentration obtained from the MODIS-Aqua satellite sensors in Fig. 8 reveals the rim current structure described above, with a maximum of chlorophyll within the coastal jet outlining the southwestern coast of the SCS, then along the continental slope bounding the eastern continental shelf, almost exactly along the 100–300 m contours of bathymetry shown in Fig. 7. The other place where a maximum of chlorophyll concentration is along a line extending west from the eastern shelf slope region, which is reminiscent of the jet between the cyclonic and anticyclonic gyres of the western SCS found in our seasonal simulations. High chlorophyll values are found trapped in two anticyclonic eddies along the southern coast, similar to the small vortices found there in our simulations.

Caspian Sea ocean model

M. Gunduz E. Özsoy

Title Page

Abstract

Introduction

Conclusions

References

Tables

Figures

◀

▶

◀

▶

Back

Close

Full Screen / Esc

Printer-friendly Version

Interactive Discussion



6 Upwelling

In summer through early fall there is continuous upwelling along the eastern coast of the Caspian Sea, studied by numerous authors (Baidin and Kosarev, 1986; Kosarev, 1975, 1990; Terziev et al., 1992; Sur et al., 2000). Satellite SST data often show relatively colder waters along the coast and filaments penetrating offshore from the upwelling region. The upwelling region extends from 41° to 44° N along the eastern coast with temperature anomaly of 2–3 °C in a region extending 5–20 km from the coast. The upwelling at the central part of the eastern coast appears more active in this image, but a review of similar data shows that the upwelling region shifts to the north or south during other times. The eastern coast upwelling is closely related with the predominant northerly winds in summer. The upwelling distribution evidently changes with the wind intensity and direction.

Figure 9 shows snapshots of model SST at days 200, 215, 230, 245 and 260 of the model annual cycle, at the upwelling region along the eastern coast of the Caspian Sea. Mesoscale dynamic features such as cold filaments, single and mushroom shaped dipole eddies are often evident in the SST patterns throughout the whole model year. The upwelling at times covers the entire eastern coast, while at other times (e.g. day 245), it almost vanishes. Irregularities along the coast, such as headlands and changes in orientation or slope of the complex topography affect the structure of the upwelled waters. Filaments of upwelled cold water reach the interior of the basin following the generally westward Ekman drift currents at the surface. Upwelling features in the model simulated SST are consistent with satellite observations based on the Pathfinder SST data set (not shown).

Compared to the other biologically active upwelling regions of the world ocean, plankton blooms with high chlorophyll concentration peculiarly are not evident in satellite data of the upwelling region along the eastern coast of the Caspian Sea.

An important consequence of Caspian Sea upwelling is the advection of high salinity water onto the shelf by compensation currents along the coast, creating favorable

OSD

11, 259–292, 2014

Caspian Sea ocean model

M. Gunduz E. Özsoy

Title Page

Abstract

Introduction

Conclusions

References

Tables

Figures

◀

▶

◀

▶

Back

Close

Full Screen / Esc

Printer-friendly Version

Interactive Discussion



conditions (pre-conditioning) for dense water formation during the later winter period, which then leads to intense slope convection that can ventilate the deeper waters of the Middle Caspian Sea.

7 Dense water formation

Ventilation of the deep waters of the Caspian Sea occurs through a series of complex processes. The rate of formation of dense water is controlled by the rate of cooling in the shallow continental shelf areas in the northern part of the Caspian Sea, ice formation in the North Caspian Sea, saline water ejection by ice, the background stratification and incidence of fronts, fresh water input, surface fluxes and meso-scale circulation. The fate of the sinking dense water depends on topography through its influence on the circulation. As dense bottom currents flow down the continental slope and into the sea interior, they entrain lower density overlying water, thus becoming relatively less negatively buoyant, influencing interior ocean properties (Papadakis et al., 2003).

Dense water formation contributes to renewal of the deep water, and thereby affects the circulation of the sea. The mechanism for dense water formation is not clear in the Caspian Sea. Rodionov (1994) has suggested two possible mechanisms for sinking of dense water: (1) in summer, evaporation increases the density of sea water at the surface, which then sinks deeper, especially along the eastern coast, (2) in winter, salt ejection by freezing results in saline surface water in the NCS which could be incorporated into the dense water formed. In addition, surface waters flowing northward along the eastern coast of the MCS come into contact with the ice on the northern slopes of the MCS, become denser by cooling and sink to greater depths of the MCS (Ferronsky et al., 2003). Kosarev and Yablonskaya (1994) have also noted that the conditions for development of winter-time vertical motions are more favorable along the eastern coast compared to other regions.

Based on two cruises performed in September 1995 and September 1996 (Peeters et al., 2000) have suggested a similar mechanism for dense water formation, whereby

Title Page

Abstract

Introduction

Conclusions

References

Tables

Figures

◀

▶

◀

▶

Back

Close

Full Screen / Esc

Printer-friendly Version

Interactive Discussion



water transported north along the eastern part of the Caspian Sea becomes colder by encountering the ice and less saline cold water in the north and sinks to the deeper parts of the Middle Caspian Sea. Climatological data show a cold water mass with high density near the eastern coast at 44° N latitude.

5 In our model experiments we found dense water formation in the northeastern part of the MCS as speculated by former authors. Figure 10 shows the evolution of density of the deepest depth over the dense water formation site. Beginning with January, day 20, dense water is evident along the eastern coast of the sea, tighten towards the coast. The density of waters along the eastern coast gradually increase in day 40 and begin
10 to move to the interior of the sea. In day 60 any day 80 dense water flows down at continental slope and fill the interior of the sea. Beginning with the April the density of deepest depth become much lesser during its course, and dense water generation finished along the eastern coast.

8 Role of the rivers

15 With fresh water inputs from a large river such as the Volga, the river buoyancy contribution is commonly expected to be an important driver of circulation. In the case of the Caspian Sea, the observed southward flow along the western coast is anticipated to be a major component of this buoyancy driven circulation. To test this statement, an experiment was designed in which the river-runoff is turned off, leaving climatological
20 surface fluxes and wind stress as the only forcing.

Turning rivers off, it is found that main features of the circulation are preserved, though weaker. It is also noteworthy that not only the surface currents, but also the deeper currents decrease in intensity when the rivers are turned off. Figure 11 compares the annual mean surface currents in the MCS with and without rivers in better
25 detail. There is significant weakening of the west coast southerly jet and the Derbent anticyclone fed by this current, when the river inflow is turned off. The other feature noted in Fig. 11 is the decrease in intensity of the current near the north-eastern coast

Caspian Sea ocean model

M. Gunduz E. Özsoy

Title Page

Abstract

Introduction

Conclusions

References

Tables

Figures

◀

▶

◀

▶

Back

Close

Full Screen / Esc

Printer-friendly Version

Interactive Discussion



of the basin. The similarity of the other features with and without the river effect signify the roles of the wind and surface buoyancy forcing in maintaining these circulation features. The fresh water discharge appears primarily responsible for maintaining the pronounced southward flowing coastal jet and the anticyclone along the west coast, as well as the surface coastal jet on the eastern coast of the MCS. The effect of major rivers in the north are of consequence in the SCS: the cyclonic gyre in north-west of the SCS becomes much weaker, while the cyclonic gyre in the southeast becomes more intense and covers almost the entire basin in the case without river runoff.

9 Conclusions

A high resolution eddy-resolving hydrodynamic model was used to investigate the dynamics of the Caspian Sea circulation. The model, forced by climatological mean seasonal atmospheric forcing and river inputs of fresh water, successfully reproduces the rather well known features of the Caspian Sea circulation and reveals the meso-scale variability of the circulation.

Based on the model results, the circulation at the surface, at intermediate depth below the mixed layer, and at deeper levels are schematized in Fig. 12 based on the annual circulation patterns presented in Fig. 3. These schematic patterns were constructed by eliminating currents of magnitude greater than 2.5 cm s^{-1} at the surface, 1 cm s^{-1} at intermediate depth, and 0.3 cm s^{-1} at the deep levels, respectively, and using the remaining current vectors.

The surface circulation (Fig. 12a) consists of narrow coastal jets originating in the north and flowing south along western and eastern coasts. Part of the flow escaping from these jets near headlands are incorporated in other elements of the circulation. In this way, the coastal jets and the anticyclonic/cyclonic gyres in the individual basins are interconnected by thin streams of currents which follow the coast and the continental slope. In a number of cases a strong current following a stream is diverted by a nearby feature, running opposite to its first orientation: for example at the headland on the

OSD

11, 259–292, 2014

Caspian Sea ocean model

M. Gunduz E. Özsoy

Title Page

Abstract

Introduction

Conclusions

References

Tables

Figures

◀

▶

◀

▶

Back

Close

Full Screen / Esc

Printer-friendly Version

Interactive Discussion



Caspian Sea ocean model

M. Gunduz E. Özsoy

Title Page

Abstract

Introduction

Conclusions

References

Tables

Figures

◀

▶

◀

▶

Back

Close

Full Screen / Esc

Printer-friendly Version

Interactive Discussion



northeastern coast, along the western coast in the proximity of the anticyclonic gyre of the MCS, at the southern coast and on the eastern side of the dipole in the SCS.

The intermediate depth circulation, Fig. 12b, is much simpler, and consists of the anticyclone in the MCS and the cyclone/anticyclone pair in the SCS, and a south to north current along the main eastern basin topographic slope (which extends to the mid-basin in the SCS and appears closer to the eastern coast in the MCS). This northward current then interconnects to the cyclonic/anticyclonic cells on the western side of the basin.

The deep circulation, Fig. 12c, consists only of the anticyclonic cell in the MCS and the cyclonic/anticyclonic pair in the SCS, without appreciable slope currents joining them. Overall, the three major cells of circulation and shelf currents displayed in Fig. 12 appear to have significant barotropic components.

Acknowledgements. We would like to thank R. Ibrayev for numerous discussions and data support. The numerical HYCOM simulations were performed under the National Center for High Performance Computing (NCHPC) at the Istanbul Technical University, Istanbul Turkey. This research is funded by Multidisciplinary Analysis of the Caspian Sea Ecosystem (MACE) project.

References

- Arpe, K. and Roeckner, E.: Simulation of the hydrological cycle over Europe: model validation and impacts of increasing greenhouse gases, *Adv. Water Resour.*, 23, 105–119, 1999. 260
- Arpe, K., Bengtsson, L., Golitsyn, G. S., Mokhov, I. I., Semenov, V. A., and Sporyshev, P. V.: Connection between Caspian sea level variability and ENSO, *Geophys. Res. Lett.*, 27, 2693–2696, 2000. 260
- Baidin, S. S. and Kosarev, A. N. (Eds.): *The Caspian Sea, Hydrology and Hydrochemistry*, Nauka, 1986. 261, 272
- Bengtsson, L.: Climate modelling and prediction, *Achievements and challenges*, in: WMO/IOC/ICSU Conference On The WCRP Climate Variability And Predictability Study (CLIVAR), UNESCO, Paris, 1998. 260

Caspian Sea ocean model

M. Gunduz E. Özsoy

Title Page

Abstract

Introduction

Conclusions

References

Tables

Figures

◀

▶

◀

▶

Back

Close

Full Screen / Esc

Printer-friendly Version

Interactive Discussion



- Bleck, R.: An oceanic general circulation model framed in hybrid isopycnic-Cartesian coordinates, *Ocean Model.*, 4, 55–88, 2002. 264
- Bleck, R.: On the use of hybrid vertical coordinates in ocean circulation modeling, in: *Ocean Weather Forecasting: an Integrated View of Oceanography*, edited by: Chassignet, E., and Verron, J., 109–126, international Summer School of Oceanography, Agelonde in Lalonde-Les Maures, Agelonde, France, 20 September–1 October 2004, 2006. 264
- Bondarenko, A. L. (Ed.): *Currents of the Caspian Sea and Formation of Salinity of the Waters of the North Part of the Caspian Sea*, Nauka, Moscow, 1993. 261, 262
- Chassignet, E., Smith, L., Halliwell, G., and Bleck, R.: North Atlantic simulations with the Hybrid Coordinate Ocean Model (HYCOM): impact of the vertical coordinate choice, reference pressure, and thermobaricity, *J. Phys. Oceanogr.*, 33, 2504–2526, 2003. 264
- Chen, C., Zheng, L., and Blanton, J.: Physical processes controlling the formation, evolution, and perturbation of the low-salinity front in the inner shelf off the southeastern United States: a modeling study, *J. Geophys. Res.-Oceans*, 104, 1259–1288, 1999. 261
- Dumont, H.: The Caspian Lake: history, biota, structure, and function, *Limnol. Oceanogr.*, 43, 44–52, 1998. 261
- Ferronsky, V., Brezgunov, V., Vlasova, L., Polyakov, V., Froehlich, K., and Rozansky, K.: Investigation of Water-Exchange Processes in the Caspian Sea on the Basis of Isotopic and Oceanographic Data, *Water Resour.*, 30, 10–22, 2003. 273
- Ibrayev, R., Sarkisyan, A., and Trukhchev, D.: Seasonal variability of the circulation of the Caspian Sea reconstructed from mean multi-year hydrological data, *Izvestiya, Atmos. Ocean. Phys.*, 37, 103–111, 2001. 265
- Ibrayev, R. A., Özsoy, E., Schrum, C., and Sur, H. Í.: Seasonal variability of the Caspian Sea three-dimensional circulation, sea level and air-sea interaction, *Ocean Sci.*, 6, 311–329, doi:10.5194/os-6-311-2010, 2010. 262
- Kara, A., Hurlburt, H., Wallcraft, A., and Bourassa, M.: Black sea mixed layer sensitivity to various wind and thermal forcing products on climatological time scales, *J. Climate*, 18, 5266–5293, 2005. 264
- Kelly, K. A., Thompson, L., Cheng, W., and Metzger, E. J.: Evaluation of HYCOM in the Kuroshio Extension region using new metrics, *J. Geophys. Res.-Oceans*, 112, C01004, doi:10.1029/2006JC003614, 2007. 264
- Klevtsova, N. (Ed.): *Sea current regime near east coast of the middle and south Caspian basin*, vol. 3 of 4, Proceeding of Hydro-meteo observatory of Baku, 1967. 261

Caspian Sea ocean model

M. Gunduz E. Özsoy

Title Page

Abstract

Introduction

Conclusions

References

Tables

Figures

◀

▶

◀

▶

Back

Close

Full Screen / Esc

Printer-friendly Version

Interactive Discussion



- Knysh, V., Ibrayev, R., Korotaev, G., and Inyushina, N.: Seasonal variability of climatic currents in the Caspian Sea reconstructed by assimilation of climatic temperature and salinity into the model of water circulation, *Izvestiya, Atmos. Ocean. Phys.*, 44, 236–249, 2008. 262, 263
- Kosarev, A. (Ed.): *Hydrology of the Caspian and Aral Seas*, Mosk Gos Univ, Moscow, 1975. 272
- 5 Kosarev, A. (Ed.): *The Caspian Sea, Water structure and dynamics*, Nauka, Moscow, 1990. 272
- Kosarev, A. and Yablonskaya, E.: *The Caspian Sea*, SPB Academic Publishing, The Hague, 1994. 261, 262, 264, 266, 273
- 10 Kourafalou, V., Oey, L., Wang, J., and Lee, T.: The fate of river discharge on the continental shelf, 1. Modeling the river plume and the inner shelf coastal current, *J. Geophys. Res.-Oceans*, 101, 3415–3434, 1996. 261
- Lazure, P. and Jegou, A.-M.: 3-D modelling of seasonal evolution of Loire and Gironde plumes on Biscay Bay continental shelf, *Oceanol. Acta*, 21, 165–177, 1998. 261
- 15 Lednev, V. A. (Ed.): *Currents of the Northern and Central Parts of the Caspian Sea*, Moscow, 1943. 262, 267
- Özsoy, E.: Sensitivity to global change in temperate Euro-Asian Seas (The Mediterranean, Black Sea and Caspian Sea): a review, in: *The Eastern Mediterranean as a Laboratory Basin for the Assessment of Contrasting Ecosystems*, edited by: Malanotte-Rizzoli, P. and Eremeev, V., vol. 51 of NATO Science Series, 281–300, Springer Netherlands, 1999. 260
- 20 Özsoy, E., Kubilay, N., Nickovic, S., and Moulin, C.: A hemispheric dust storm affecting the Atlantic and Mediterranean in April 1994: Analyses, modeling, ground-based measurements and satellite observations, *J. Geophys. Res.-Atmos.*, 106, 18439–18460, 2001. 260
- Papadakis, M., Chassignet, E., and Hallberg, R.: Numerical simulations of the Mediterranean sea outflow: impact of the entrainment parameterization in an isopycnic coordinate ocean model, *Ocean Model.*, 5, 325–356, 2003. 273
- 25 Peeters, F., Kipfer, R., Achermann, D., Hofer, M., Aeschbach-Hertig, W., Beyerle, U., Imboden, D., Rozanski, K., and Frohlich, K.: Analysis of deep-water exchange in the Caspian Sea based on environmental tracers, *Deep-Sea Res. Pt. I.*, 47, 621–654, 2000. 267, 273
- 30 Rachev, N. H. and Stanev, E. V.: Eddy processes in semiencloded seas: a case study for the Black Sea, *J. Phys. Oceanogr.*, 27, 1581–1601, 1997. 269
- Rodionov, S.: *Global and regional Climate Interaction: the Caspian Sea Experience*, Kluwer Academic Publ., Dordrecht, the Netherlands., 1994. 260, 273

Caspian Sea ocean model

M. Gunduz E. Özsoy

Title Page

Abstract

Introduction

Conclusions

References

Tables

Figures

◀

▶

◀

▶

Back

Close

Full Screen / Esc

Printer-friendly Version

Interactive Discussion



- Sarkisyan, A. S., Zaripov, B. R., Kosarev, A. N., and Rzhaplinski, D. G.: Diagnostic calculations of currents in the Caspian Sea., *Izvestiya, Atmos. Ocean. Phys.*, 12, 1106–1110, 1976. 262
- Stockman, W.: Investigation of current kinematics at the western shore of the central part of the Caspian Sea., vol. 1, Transactions of the Azerbaidjan Scientific-Investigative Fishery station, 1938. 261
- 5 Sur, H. I., Özsoy, E., and Ibrayev, R.: Chapter 16 Satellite-derived flow characteristics of the Caspian Sea, in: *Satellites, oceanography and society*, edited by: Halpern, D., vol. 63 of Elsevier Oceanography Series, 289–297, Elsevier, 2000. 262, 272
- Terziev, F., Kosarev, A., and Keromov, A., eds.: *Hydrometeorology and hydrochemistry of Seas*, vol. VI, The Caspian Sea, Gidrometeoizdat, Leningrad, 1992. 262, 272
- 10 Trukhchev, D., Kosarev, A., Ivanova, D., and Tuzhilkin, V.: Numerical Analysis of the general circulation in the Caspian Sea, *Comptes Rendus de l'Academie Bulgare des Sciences*, 35–38, 1995. 262, 267
- Tsytsarev, A. N., ed.: Peculiarities of drift currents near Kura river mouth., 5, *Proceeding of Baku Hydrometeobservatory*, 1967. 261
- 15 Tuzhilkin, V., Kosarev, A., Trukhchev, D., and D. P., I.: Seasonal features of General Circulation in the Caspian Deep-water, *Meteorol. Hydrol.*, 1, 91–99, 1997. 262, 267
- Vorosmarty, C., Sharma, K., Fekete, B., Copeland, A., Holden, J., Marble, J., and Lough, J.: The storage and aging of continental runoff in large reservoir systems of the world, *Ambio*, 26, 210–219, 1997. 264
- 20 Wallcraft, A., Kara, A., Hurlburt, H., and Rochford, P.: The NRL Layered Global Ocean Model (NLOM) with an embedded mixed layer submodel: formulation and tuning, *J. Atmos. Ocean Tech.*, 20, 1601–1615, 2003. 265

Caspian Sea ocean model

M. Gunduz E. Özsoy

Table 1. Climatological mean flow values obtained from RivDIS (see online at <http://daac.ornl.gov/rivdis/>), for the river discharge into the Caspian Sea.

	Volga ($\text{m}^3 \text{s}^{-1}$)	Kura ($\text{m}^3 \text{s}^{-1}$)	Ural ($\text{m}^3 \text{s}^{-1}$)
Jan	3917.5	467.9	60.9
Feb	3960.2	493.9	56.0
Mar	4032.8	553.0	70.1
Apr	7488.5	813.3	899.5
May	24 021.5	1067.2	1377.3
Jun	20 075.3	850.8	409.7
Jul	8163.6	451.7	198.5
Aug	5590.6	313.7	131.9
Sep	5036.9	326.7	105.3
Oct	5358.7	387.9	98.4
Nov	5450.0	423.8	90.8
Dec	3948.0	461.0	63.4

Title Page

Abstract

Introduction

Conclusions

References

Tables

Figures

◀

▶

◀

▶

Back

Close

Full Screen / Esc

Printer-friendly Version

Interactive Discussion



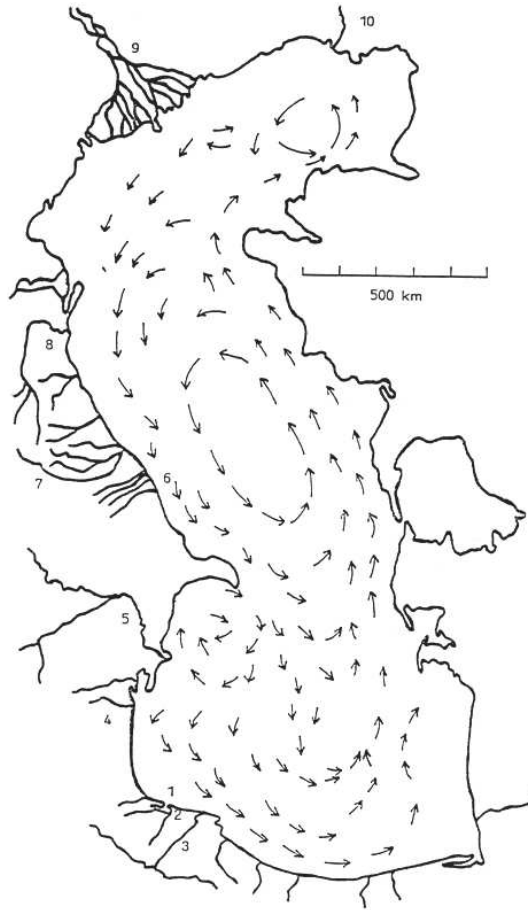


Fig. 1. Schematic representation of the Caspian Sea currents (Lednev, 1943).

Caspian Sea ocean model

M. Gunduz E. Özsoy

Title Page

Abstract Introduction

Conclusions References

Tables Figures

◀ ▶

◀ ▶

Back Close

Full Screen / Esc

Printer-friendly Version

Interactive Discussion



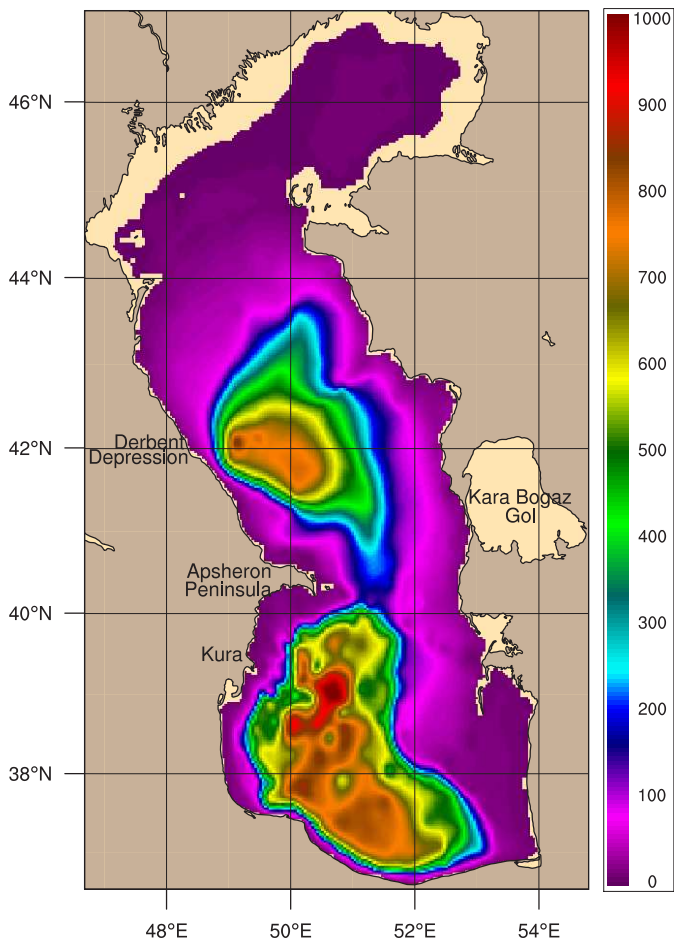


Fig. 2. The Caspian Sea model bathymetry.

Caspian Sea ocean model

M. Gunduz E. Özsoy

Title Page

Abstract Introduction

Conclusions References

Tables Figures

◀ ▶

◀ ▶

Back Close

Full Screen / Esc

Printer-friendly Version

Interactive Discussion



Caspian Sea ocean model

M. Gunduz E. Özsoy

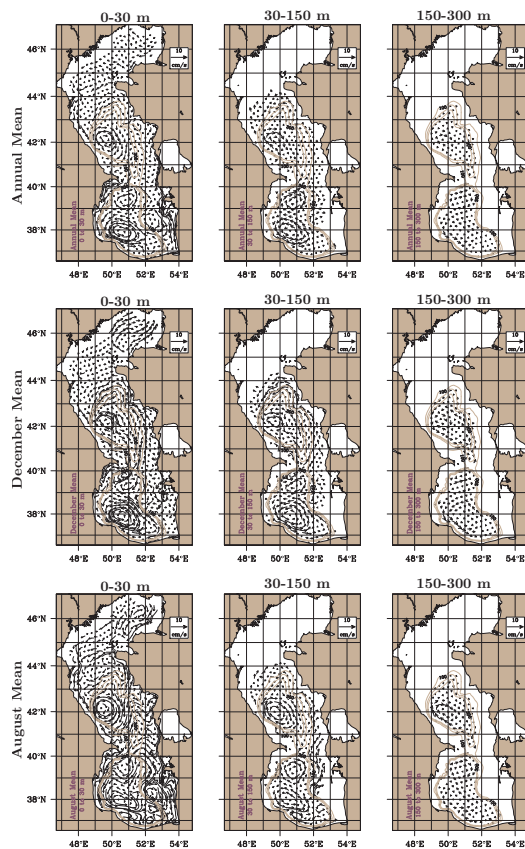


Fig. 3. Model derived mean currents (cm s^{-1}) from control run averaged over depth intervals of 0–30 m, 30–150 m and 150–300 m. Countour lines shows the 100, 200, 300 m bathymetry contours. Upper: annual, middle: December, lower: August.

Title Page

Abstract

Introduction

Conclusions

References

Tables

Figures

◀

▶

◀

▶

Back

Close

Full Screen / Esc

Printer-friendly Version

Interactive Discussion



Caspian Sea ocean model

M. Gunduz E. Özsoy

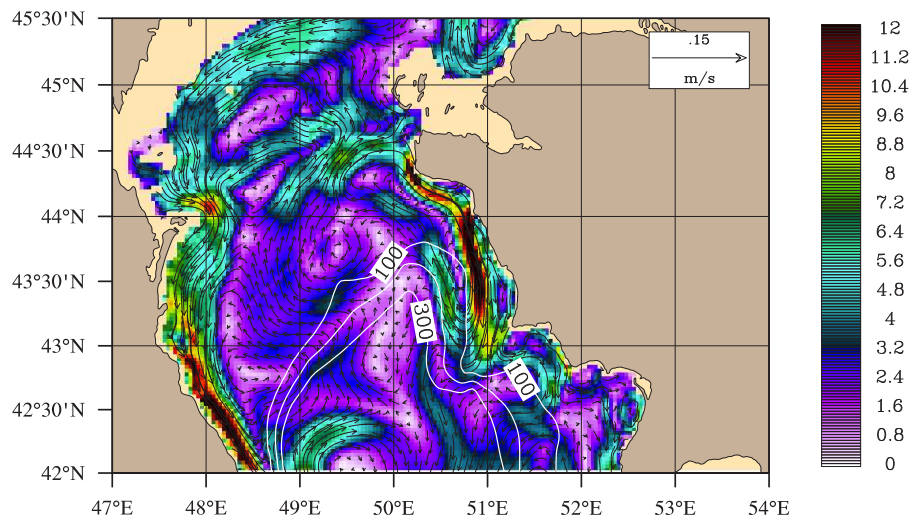


Fig. 4. Model derived current in July over the MCS. The southward flow along the north-eastern coast of the MCS is evident in this figure.

[Title Page](#)[Abstract](#)[Introduction](#)[Conclusions](#)[References](#)[Tables](#)[Figures](#)[◀](#)[▶](#)[◀](#)[▶](#)[Back](#)[Close](#)[Full Screen / Esc](#)[Printer-friendly Version](#)[Interactive Discussion](#)

Caspian Sea ocean model

M. Gunduz E. Özsoy

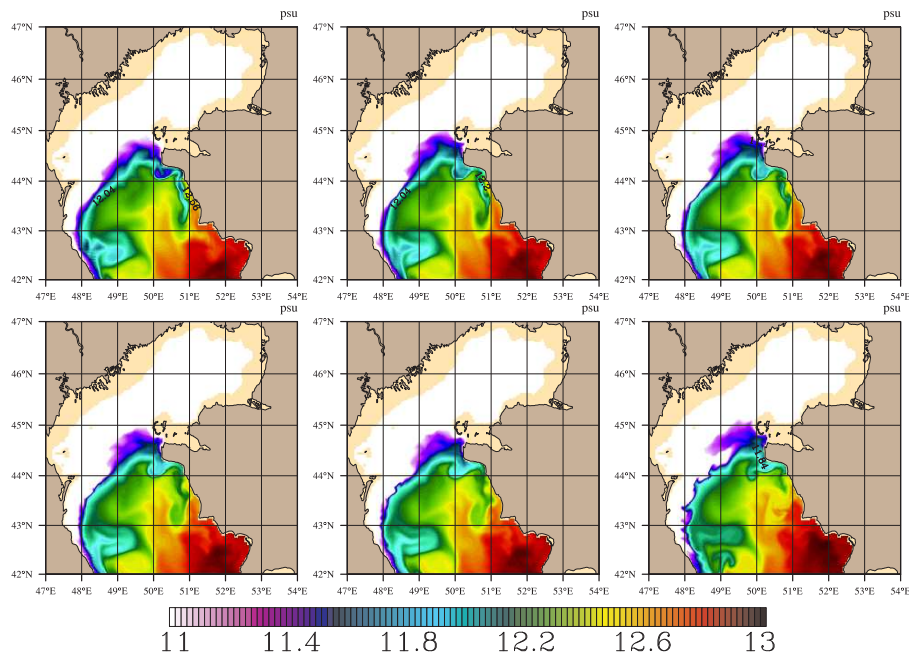


Fig. 5. Sea Surface Salinity (SSS) for a series of model days upper: 210, 212, 213 lower: 214, 215, 221.

[Title Page](#)[Abstract](#)[Introduction](#)[Conclusions](#)[References](#)[Tables](#)[Figures](#)[◀](#)[▶](#)[◀](#)[▶](#)[Back](#)[Close](#)[Full Screen / Esc](#)[Printer-friendly Version](#)[Interactive Discussion](#)

Caspian Sea ocean model

M. Gunduz E. Özsoy

Title Page

Abstract

Introduction

Conclusions

References

Tables

Figures

◀

▶

◀

▶

Back

Close

Full Screen / Esc

Printer-friendly Version

Interactive Discussion

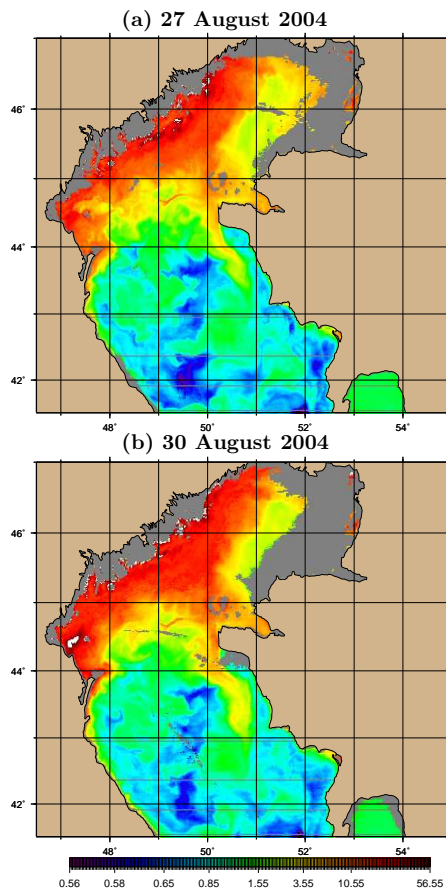


Fig. 6. Chlorophyll concentration (in mg m^{-3}) on **(a)** 27 August 2004 **(b)** 30 August 2004. The chlorophyll concentration contours are plotted with different colours and intervals for a better visualization of structure.

Caspian Sea ocean model

M. Gunduz E. Özsoy

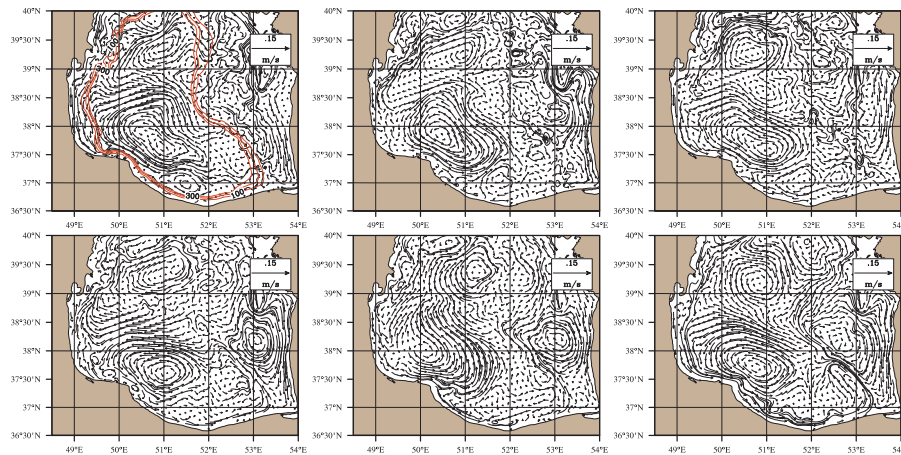


Fig. 7. The evolution of the flow field in the SCS during upper: 195, 225, 255 lower: 285, 315, 345 days of the model days, the red line in the first figure shows the 100, 200, 300 m bathymetry countour.

Title Page

Abstract

Introduction

Conclusions

References

Tables

Figures

◀

▶

◀

▶

Back

Close

Full Screen / Esc

Printer-friendly Version

Interactive Discussion



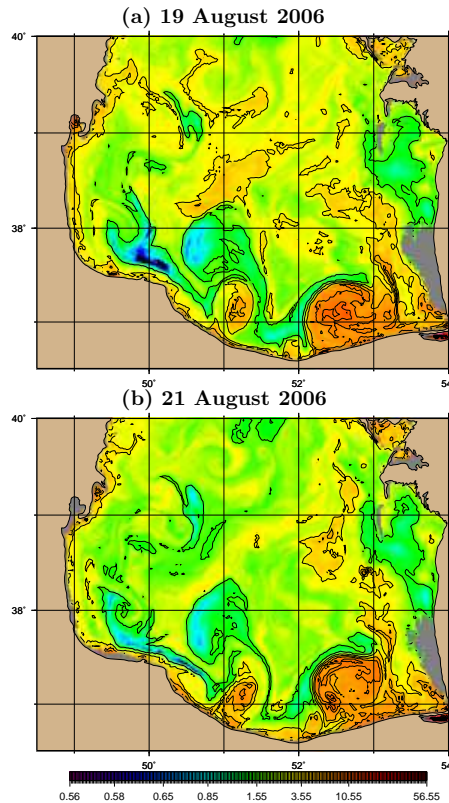


Fig. 8. Chlorophyll concentration (in mgm^{-3}) on **(a)** 19 August 2006 **(b)** 21 August 2006. The chlorophyll concentration contours are plotted with different colours and intervals for a better visualization of structure.

Caspian Sea ocean model

M. Gunduz E. Özsoy

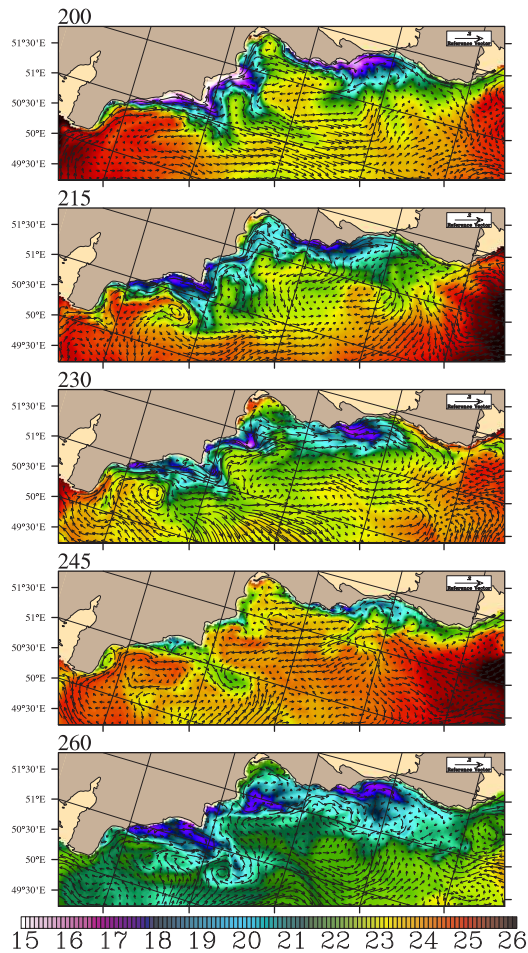


Fig. 9. Snapshot of the model SST of the 8th model year along the eastern coast of the Sea. The model days are shown at upper left side of the each figure.

[Title Page](#)[Abstract](#)[Introduction](#)[Conclusions](#)[References](#)[Tables](#)[Figures](#)[◀](#)[▶](#)[◀](#)[▶](#)[Back](#)[Close](#)[Full Screen / Esc](#)[Printer-friendly Version](#)[Interactive Discussion](#)

Caspian Sea ocean model

M. Gunduz E. Özsoy

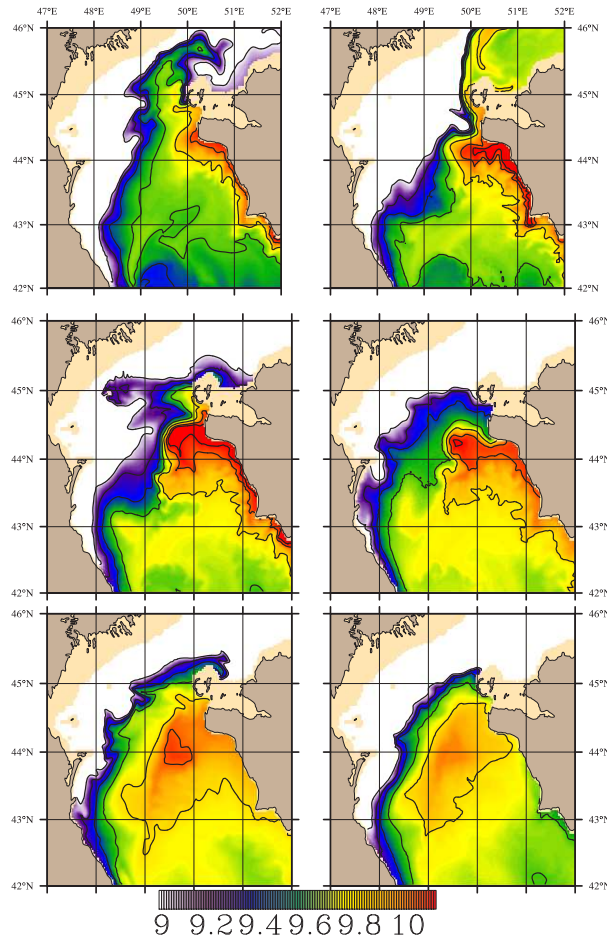


Fig. 10. Density of deepest depth at model days upper: 2, 20 middle: 40, 60 lower: 80, 92. White areas shows the density less than 9.

Title Page

Abstract Introduction

Conclusions References

Tables Figures

◀ ▶

◀ ▶

Back Close

Full Screen / Esc

Printer-friendly Version

Interactive Discussion



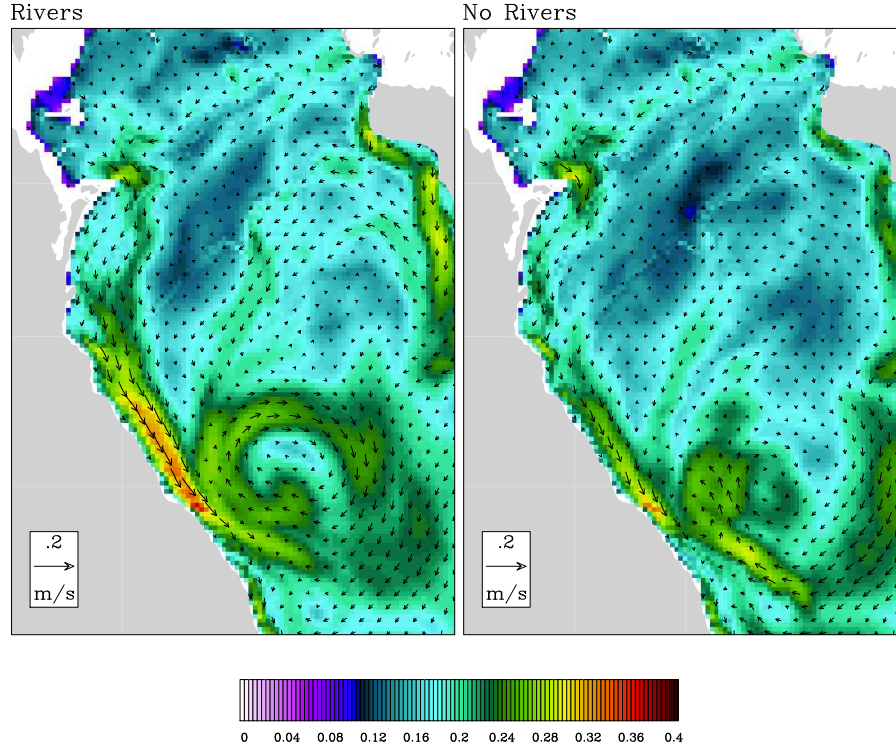


Fig. 11. Model surface velocity vector mean and rms vector amplitude over the year simulation, with rivers and without rivers. Means are denoted with arrows while rms amplitude is color contoured. Every fourth vector is shown in the along-shore and across-shore direction.

Title Page

Abstract

Introduction

Conclusions

References

Tables

Figures

◀

▶

◀

▶

Back

Close

Full Screen / Esc

Printer-friendly Version

Interactive Discussion



Caspian Sea ocean model

M. Gunduz E. Özsoy

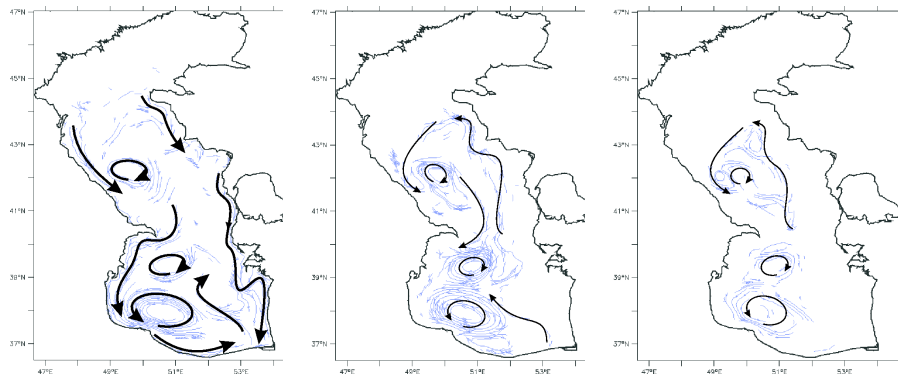


Fig. 12. Schematic representation of annual mean circulation of the Caspian Sea for the depth ranges **(a)** surface (0–10 m), **(b)** intermediate (50–100 m) **(c)** deep (200–1000 m).

Title Page

Abstract

Introduction

Conclusions

References

Tables

Figures

◀

▶

◀

▶

Back

Close

Full Screen / Esc

Printer-friendly Version

Interactive Discussion

